Surface Charge of Clean $LiNbO_3$ Z-Cut Surfaces

S. Sanna, U. Gerstmann, E. Rauls, Y. Li, M. Landmann, A. Riefer, M. Rohrmüller, N.J. Vollmers, M. Witte, R. Hölscher, A. Lücke, C. Braun, S. Neufeld, K. Holtgrewe, and W.G. Schmidt

Abstract The geometry of the polar $LiNbO_3$ (0001) surface is strongly temperature dependent. In this work the surface charge associated to various surface terminations is estimated from *first-principles* calculations. All stable terminations are found to lower the polarization charge, showing that the surface charge compensation is a major driving force for surface reconstruction.

1 Introduction

Surfaces of ferroelectric materials, in particular the lithium niobate (0001) surface (LN Z-cut), are widely exploited, e.g., for surface acoustic wave devices [1] or to grow group III nitrides with spatially varied polarity control [2]. Also artificial photosynthesis [3], photocatalytic dye decolorization [4] as well as activation of charged biomolecules [5] were demonstrated. The high surface electric fields were found to efficiently pole electro-optic polymers [6] and to lead to the reversible fragmentation and self-assembling of nematic liquid crystals [7]. Of particular interest is the possibility to switch the surface polarization, and thus the surface chemistry [8].

Given these exciting applications, surprisingly little is known about the microscopic LN surface structure. Only very recently atomically resolved Atomic Force Microscopy (AFM) images of LN Z-cut could be obtained [9]. While no surface reconstruction was found for samples annealed at 1,270 K, a series of structural transformations, including a $\sqrt{7} \times \sqrt{7}$ R19° surface reconstruction [10] were found at samples annealed at lower temperatures. This was interpreted as the result of different charge compensation mechanisms: At low temperatures foreign adsorbates compensate the surface polarization charge. If the temperature is sufficiently high to drive off the adsorbates, surface reconstructions form that lower the electrostatic energy. Finally, at temperatures close to the Curie temperature of LN, the sponta-

S. Sanna • U. Gerstmann • E. Rauls • Y. Li • M. Landmann • A. Riefer • M. Rohrmüller • N.J. Vollmers • M. Witte • R. Hölscher • A. Lücke • C. Braun • S. Neufeld • K. Holtgrewe • W.G. Schmidt (✉)
Lehrstuhl für Theoretische Physik, Universität Paderborn, 33095 Paderborn, Germany
e-mail: W.G.Schmidt@upb.de

W.E. Nagel et al. (eds.), *High Performance Computing in Science and Engineering '14*, DOI 10.1007/978-3-319-10810-0_12

neous polarization, and thus the surface charge, are strongly reduced and the surface reconstructions are quenched [10].

In the present work an approximate method to estimate the surface charge within the density-functional theory (DFT) calculations using periodic boundary conditions (PBCs) is proposed and used in order rationalize the structural models proposed in Ref. [10] in terms of surface charge compensation.

2 Methodology

As in our previous studies on $LiNbO_3$ surfaces [10–13], we perform self-consistent DFT calculations using the Vienna Ab initio Simulation Package (VASP) [14]. All-electron projector-augmented wave potentials within the PW91 formulation of the generalized gradient approximation (GGA) [15] are used. A plane-wave basis set including waves up to an energy of 400 eV is used to expand the electronic orbitals. The atomic positions have been determined minimizing the Hellmann-Feynman forces acting on the single atoms to be below 0.02 eV/Å. A $4 \times 4 \times 1$ Γ-centered Monkhorst-Pack [16] k-point mesh was used to carry out the integration in the Brillouin zone for the simulation of truncated bulk, unreconstructed and $\sqrt{3} \times \sqrt{3}$ reconstructed surfaces. A $2 \times 2 \times 1$ k-point mesh was chosen to sample the much smaller Brillouin zone of the slabs modeling $\sqrt{7} \times \sqrt{7}$ reconstructed surfaces.

VASP offers highly customizable parallelization schemes, which allow for performance optimization on different computational architectures. In particular, parallelization (and data distribution) over bands, parallelization (and data distribution) over plane wave coefficients, as well as parallelization over k-points (no data distribution) are implemented. All of them have to be used at the same time on massively parallel systems or modern multi-core machines, in order to obtain high efficiency. The holds obviously for the HLRS CRAY XE6, the main computational resource used for this project. The performance of the CRAY XE6 in combination with the available parallelization routines has been tested and optimized. Thereby a $LiNbO_3$ slab with C_1 symmetry containing 361 atoms for a total of 2,174 electrons distributed over 1,334 orbitals serves as a realistic test system. All tests have been performed using the VASP Version 5.3.2 and employ a $4 \times 4 \times 4$ k-point mesh, corresponding to 36 irreducible k-points in the Brillouin zone.

The first step of the parallelization procedure is the distribution of the workload related to each orbital on a certain number of cores. Several choices are possible. The simplest option (and default strategy) is to treat one orbital by one core, implying distribution over plane wave coefficients only: all cores will work on every individual band, by distributing the plane wave coefficients over all cores. This is the optimal setting for machines with a single core per node and small communication bandwidth but performs rather inefficiently on the HRLS CRAY. This mode is characterized by heavy memory requirements, as the non-local projector functions must be stored entirely on each core. Furthermore, substantial

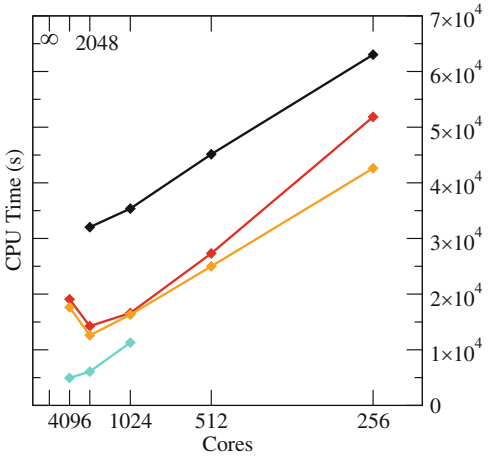

Fig. 1 CPU time on the HRLS CRAY XE6 for the self consistent calculation of the electronic structure of a $LiNbO_3$ slab within different parallelization schemes. See text for details

all-to-all communications are necessary to orthogonalize the band. This setting is usually very slow and should thus be avoided on massively parallel systems.

A better choice for system such as the HRLS CRAY is to treat each orbital with a number of cores corresponding either to the square root of all available cores (at least approximately) or to the number of cores per compute node, e.g. 32. In addition, it also significantly improves the stability of the code due to reduced memory requirements. Therefore, all tests are performed treating each orbital with a number of cores corresponding roughly to the square root of all available cores. The results of the tests on this configuration are reported in Fig. 1 (red line). This setup results in a roughly linear scaling up to 2,048 cores. Beyond this value no speedup is observed anymore. Within the described approach for parallel computing, it is possible to steer the data distribution mode. In particular, the plane wise data distribution in real space can be activated. In this way the communication related to the FFTs can be strongly reduced. Unfortunately, the resulting load balancing is worsened, so that the opportunity of switching on the plane wise data distribution must be tested on the particular computational architecture and in dependence of the number of processors. The results of the corresponding tests are shown in Fig. 1 (orange line). As expected, the advantages of the plane wise data distribution are visible for smaller numbers of processors and vanish for 1,024 cores where load-balancing problems prevail.

The VASP implementation of DFT makes heavy use of mathematical libraries, such as the (scalable) linear algebra package (Sca)LAPACK. The effect of using ScaLAPACK vs. LAPACK libraries is shown in Fig. 1 (black vs. red line). Obviously, using ScaLAPACK reduces the computational time considerably for the system studied here. Starting from the VASP Version 5.3.2 it is possible to switch on an additional parallelization over k points. Thereby the data is not distributed additionally over the k-points. In particular, it is possible to specify the number of k points that are to be treated in parallel, which has been chosen to be 8 out of

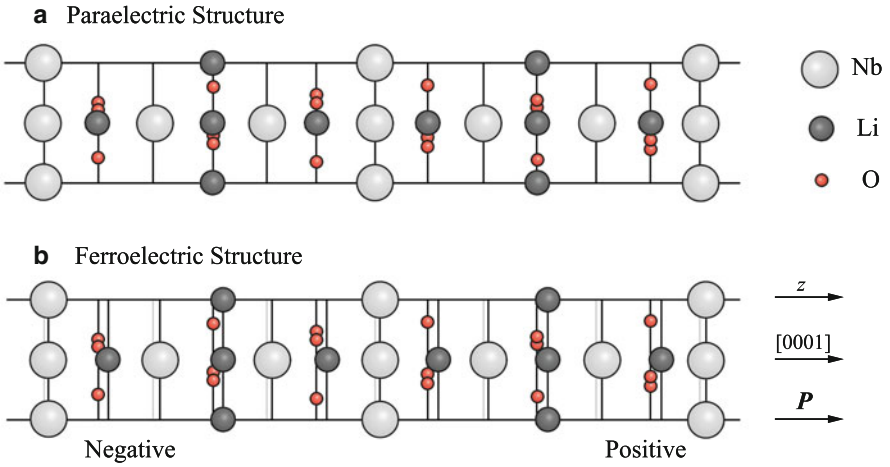

Fig. 2 Schematic representation of the paraelectric (**a**) and ferroelectric (**b**) phases of $LiNbO_3$ along the [0001] crystallographic direction. In the ferroelectric phase Li and Nb atomic layers are shifted with respect to the oxygen sublattice along the crystal *z*-axis. The *gray lines* in the ferroelectric phase represent the positions of the corresponding atomic layers in the paraelectric phase

36 in our test. Then, the set of k points is distributed over 8 groups of compute cores, in a round-robin fashion. This means that N = total-cores/8 compute cores work together on an individual k point. Of course, the number of k points that are treated in parallel must be an integer divisor of the total number of cores. Within this group of N cores that share the work on an individual k point, the usual parallelism over bands and/or plane wave coefficients applies. The results of the corresponding tests are shown in Fig. 1 (blue line). The computational time saving with respect to calculations without k point parallelization amounts to a factor of about two, thereby the scaling is roughly linear up to 4,096 cores. Summarizing, the computational time can be reduced by roughly an order of magnitude with an appropriate choice of the parallelization routines. With a combination of parallelization over bands and k-points a linear scaling at least up to 2,048 cores can be achieved.

Generally, the LN(0001) and $(000\bar{1})$ surfaces are defined as positive and negative Z-cut. The cations in the paraelectric phase are either within (Li^{+1}), or exactly between oxygen layers (Nb^{+5}), as depicted in Fig. 2. In the ferroelectric phase, the cations are shifted along the [0001] crystallographic direction with respect to the oxygen planes, causing a permanent spontaneous polarization parallel to the cationic displacement. Ferroelectric $LiNbO_3$ is thus a stacking of -Nb-O_3-Li- planes along the [0001] direction, and it is not centrosymmetric. This is an issue within the supercell approach, as the two slab surface terminations cannot be made equivalent and only relative energetic comparisons are possible. In this work we model the LN(0001) surface and all its reconstructions with 12 LN trilayers (36 atomic layers) plus surface terminations, resulting in large supercells containing from 60 atoms (for

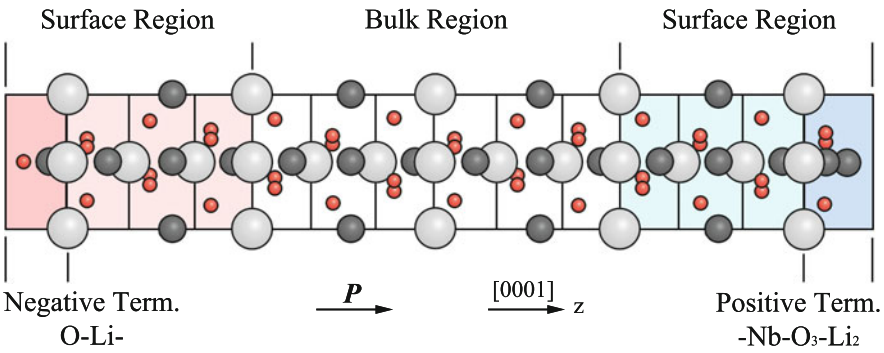

Fig. 3 Slab used to model the thermodynamically stable 1 × 1 (0001) surfaces. The surface termination and the underlying three trilayer (surface region) are free to relax, while the six central trilayer are kept frozen at their bulk positions (bulk region). The positive surface -LN(0001)- is at the right hand side, the negative surface -LN($000\bar{1}$)- at the left hand side. Atomic color coding as in Fig. 2

the simulation of the truncated bulk) up to 460 atoms for the simulation of $\sqrt{7} \times \sqrt{7}$ reconstructed surfaces. The central part of our slabs (18 atomic layers) are frozen into their ferroelectric positions, while the remaining 18 layers and the surface terminations are free to relax (see Fig. 3). This has two important advantages: On one hand, it saves some computational time. On the other hand, it defines the central part of our slab as a true bulk region, which is not affected by surface effects. A vacuum region of at least 19 Å separates the slab from its periodic images. As we shall see in the following, cells of this size are thick enough to allow for the definition of macroscopic quantities such as inner – $\boldsymbol{E}_D$ – and outer electric field – $\boldsymbol{E}_{EXT}$ – from unit cell averages of electrostatic potential $V_H(\mathbf{t})$ and charge densities $\rho(\mathbf{r})$.

The supercell approach typically makes use of periodic boundary conditions (PBCs), resulting in a vanishing macroscopic internal field $\boldsymbol{E}$ even for ferroelectrics with a spontaneous bulk polarization $\boldsymbol{P}_S^{\text{bulk}}$ (see Fig. 4a). A slab wit a net dipole moment perpendicular to the surface will give rise to an electrostatic potential as illustrated in Fig. 4b. The net dipole moment will in general have contributions from both the bulk polarization and the surface termination. Indeed, a paraelectric material with two non-equivalent surface terminations will give rise to a dipole moment too. This configuration models a surface in the artificial field caused by its neighboring periodic images. Thereby, the electrostatic potential is a continuous function. Neither internal nor external fields have direct physical interpretation as they depend on the cell geometry. Indeed, increasing the thickness of the slab or of the vacuum region the artificial fields become smaller, vanishing in the limit of infinite supercells. In order to correct for the error introduced by the artificial field in finite slabs, dipole corrections can be applied [17, 18]. The correction is introduced by adding an external dipole layer in the vacuum region of the supercell, and leads to the situation depicted in Fig. 4c, with vanishing external electric field.

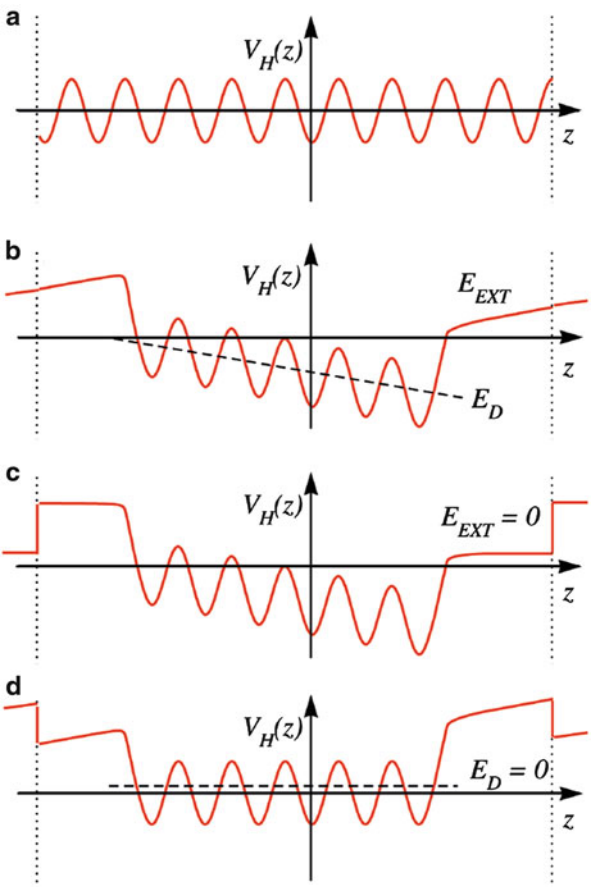

Fig. 4 Planar averaged electrostatic (Hartree) potential of ferroelectric $LiNbO_3$. (**a**) bulk supercell, (**b**) slab of truncated bulk, (**c**) with vanishing external field, and with vanishing internal electric field (**d**). Internal (or depolarization) field $\boldsymbol{E}_D$, external field $\boldsymbol{E}_{EXT}$ and slab/supercell boundaries are indicated

The electrostatic potential is now discontinuous. However, the discontinuity is localized in the vacuum region, where it is supposed not to affect the calculation. The polarization $\boldsymbol{P}$ gives rise to surface polarization charges

$$\sigma_S = \boldsymbol{P} \cdot \hat{\boldsymbol{n}}, \tag{1}$$

where $\hat{\boldsymbol{n}}$ is the surface normal.

Meyer and Vanderbilt [19] pointed out that the depolarization field $\boldsymbol{E}_D$ originating from the surface charges might be large enough to destabilize the ferroelectric state: relaxing a polarized slab under periodic boundary conditions corresponding to vanishing external electric field would result in a paraelectric structure. To overcome this problem they proposed to model polarized slabs with periodic boundary conditions corresponding to vanishing internal field, as illustrated in Fig. 4d. This boundary condition is equivalent to placing the slabs between the grounded plates

of a capacitor, and is appropriate to model very thin film geometries, where ferroelectric and dielectric properties are strongly influenced by surface effects [19].

It must be pointed out that none of the described PBCs for the electrostatic potential is intrinsically correct and universally applicable. While the vanishing internal field boundaries are the proper conditions far from the surface [19] and thus ideal for the simulation of the "bulk" of thin films, vanishing external field conditions are more appropriate to model the surface itself. Thus, the choice of the appropriate periodic boundary conditions discussed above depends on the system properties one focuses on. Being interested in surface charges, we adopt vanishing external field boundaries. To prevent the slab to relax into the paraelectric state, the central part of our slabs (18 atomic layers) are frozen into their ferroelectric positions, while the remaining 18 layers and the surface terminations are free to relax. This choice is also justified by the results of Levchenko et al. [20], who pointed out that the structural relaxation in the ferroelectric LN(0001) surfaces is limited to a few outmost atomic layers. The choice of the PBCs affects to some extent the calculated the surface charge. The difference in the surface charge calculated with – Fig. 4c – and without – Fig. 4b – dipole corrections, however, amounts to less than 0.009 C/m^2, which is two orders of magnitude lower than the charge of a LN truncated bulk. For a quantitative estimate of the surface charge, a proper treatment of the pyroelectric effect – currently neglected – will also be necessary.

As seen from Eq. 1, the polarization charge directly depends on the slab polarization. The polarization component perpendicular to the surface is a well defined quantity, and fully determines the surface charge, provided the polarization is homogeneous. The bulk macroscopic polarization is not a well defined quantity within the supercell approach, though. This is due to the fact that the choice of the supercell is not unique: different supercells characterized by different dipole moments may be chosen to model a given crystal. However, this does not affect the calculation of the surface charge related to a given termination. The macroscopic polarization can be correctly calculated as a Berry phase of the electronic orbitals within the modern theory of polarization [21, 22] with respect to a reference phase, usually the corresponding paraelectric phase:

$$\boldsymbol{P} = \int_0^1 \boldsymbol{P}'(\lambda) d\lambda = \boldsymbol{P}(1) - \boldsymbol{P}(0), \tag{2}$$

where $\lambda \in (0, 1)$ is a reaction coordinate which brings the system from the ferroelectric $\boldsymbol{P}(1)$ to the reference (paraelectric) phase $\boldsymbol{P}(0)$. Using the Berry phase approach, we have calculated the spontaneous bulk polarization of stoichiometric LN to be $0.82\,C/m^2$, in good agreement with the commonly accepted value of $0.71\,C/m^2$ [23], and with the value of $0.86\,C/m^2$ calculated in a similar manner by Levchenko et al. [20].

The surface charge σ_S of the positive and negative LN Z-cut is estimated by integrating the planar averaged polarization charge, defined as

$$\rho(z) = \frac{1}{A} \int \int_A \rho(\mathbf{r}) dxdy, \tag{3}$$

from the vacuum center (0) to the cell center (z_{cut}) in both directions

$$\sigma_S = \int_0^{z_{\text{cut}}} \rho(z) dz. \tag{4}$$

Here A is the area of the surface unit cell and $\rho(\mathbf{r})$ is the charge redistribution due to the surface formation (i.e. the difference with respect to the bulk), so that the slab is charge neutral and the integral over the whole supercell is exactly zero.

Furthermore, for the estimation of the surface charge of an ideal bulk cut, we proceed in the spirit of the Berry approach, and calculate the macroscopic surface charge with respect to a reference phase

$$\sigma_S^{cut} = \boldsymbol{P} \cdot \hat{\boldsymbol{n}} = (\boldsymbol{P_F} - \boldsymbol{P_P}) \cdot \hat{\boldsymbol{n}} = \sigma_F^{cut} - \sigma_P^{cut} \tag{5}$$

This procedure yields a surface charge which does not depend on the choice of the slab representing the ideal truncated bulk cut, provided the reference phase is chosen carefully. In our case, the reference structure is a corresponding slab of LN in the paraelectric phase. This method is applied here only for the calculation of an ideal LN bulk cut.

The integration limits of Eq. 4 need to be determined carefully: the charge density oscillations within the slab are larger than the electronic charge accumulation/depletion we want to estimate, and the value of σ_S is extremely sensitive with respect to z_{cut}. We circumvent the choice of some geometrical point z_{cut} to perform "the cut" by dividing the slab into atomic layers. In an small slab consisting of two Nb-O_3-Li tri-layers stapled along the z-direction, the lower trilayer builds the lower (negative) surface, while the upper trilayer builds the upper (positive) surface. Then, the charges of the upper (or lower) slab are summed up to calculate the surface charge. To assign a volume – and the corresponding included charge – to an atomic layer, we use the definition of Bader atomic volumes and Bader charges [24]. This procedure turns out to be very robust and only little influenced by computational parameters. Convergence tests have shown that the calculated surface charge converges quickly with respect to number of grid points in real space. Performing the calculation with or without the core electrons charge does not modify the results within the numerical accuracy.

In summary, we proceed as follows: (i) The total electronic charge of the slab representing a given termination is calculated self-consistently and then partitioned by Bader volumes into upper and lower slab half. (ii) The charge redistribution $\rho(\mathbf{r})$ of Eq. 4 is obtained by subtracting the Bader charges of the corresponding atoms in the bulk phase. (iii) Finally, the charge redistribution of the Bader volumes within the upper and within the lower slab half are summed up and yield the surface charge σ_S.

3 Results

We probe the applicability of the scheme proposed above for the truncated bulk surfaces of LN. Thereby the atomic positions are kept fixed in their bulk positions but the electron distribution is calculated self-consistently. In this case the bulk polarization represents an upper bound of the calculated surface charge since the latter may be partially compensated by the electron transfer through the slab. Considering ferroelectric LN as a stacking of Nb-O_3-Li atomic layers along the [0001] crystallographic direction, three non equivalent atomic cuts can be discriminated. Cutting the crystal above a Li layer (cut 1 in Fig. 5), the slab representing the crystal will be a succession of Nb-O_3-Li trilayers. Cutting the crystal above a Nb layer, the slab will be a succession of O_3-Li-Nb trilayers (cut 2 in Fig. 5). Finally, cutting the crystal above an oxygen layer, the slab will be a succession of Li-Nb-O_3 trilayers (cut 3 in Fig. 5). Twelve trilayers are used for the calculations. For the sake of simplicity, we only consider slabs containing an integer number of LN formula units.

The slabs built to model these cuts are characterized by very different electric dipole moments, both in magnitude and direction, resulting in three different surface charge values σ_F^{cut}. The surface charge of the different cuts has been calculated as described by Eq. 4, and the result are reported in Table 1. However, the total surface

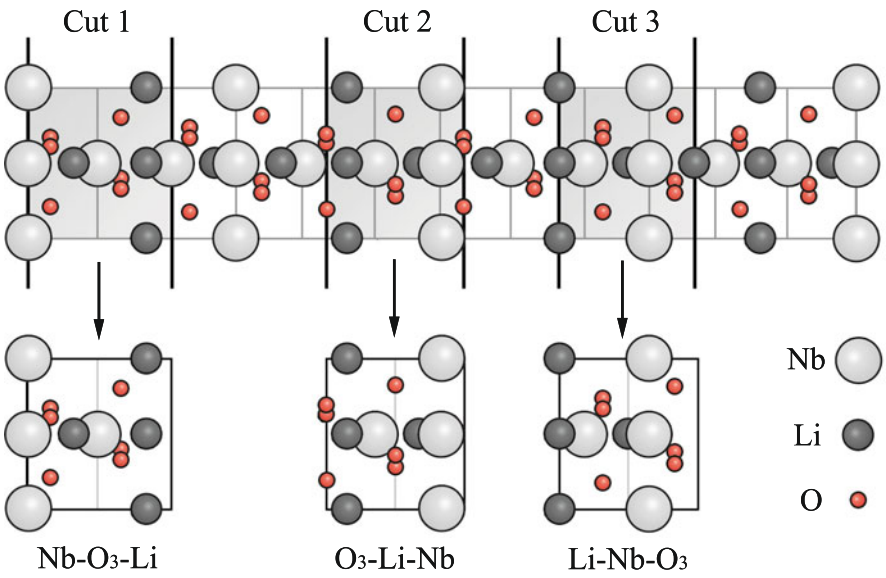

Fig. 5 Ferroelectric bulk $LiNbO_3$ can be cut perpendicularly to the [0001] direction at three non-equivalent planes, resulting in a Li, O_3, and Nb termination (Cut 1, Cut 2 and Cut 3 in the picture). Different cuts are modeled by slabs with different electric dipole moment, both in size and direction. Only slabs containing an integer number of LN formula units are considered

Table 1 Calculated surface charge ($e/(1 \times 1)$ unit cell) of the positive Z-cut for a ferroelectric slab (σ_F^{cut}), for the corresponding reference (paraelectric) phase (σ_P^{cut}) and the value σ_S^{cut} calculated with Eqs. 4 and 5. See Fig. 5 for cut definitions

	Cut 1	Cut 2	Cut 3
σ_F^{cut}	−0.66	1.95	−1.64
σ_P^{cut}	−1.31	1.31	−2.30
σ_S^{cut}	0.65	0.64	0.66

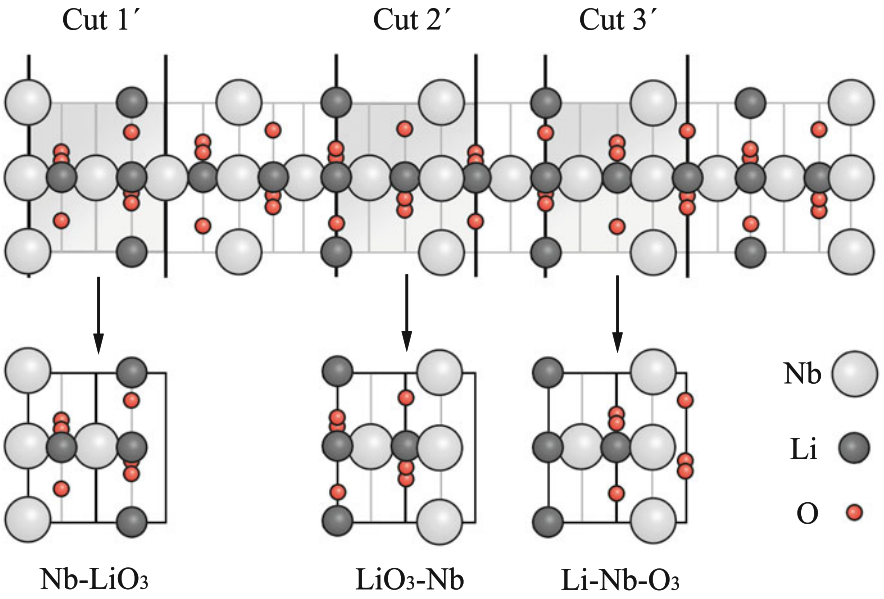

Fig. 6 Paraelectric bulk $LiNbO_3$ can be cut perpendicularly to the [0001] direction at two non-equivalent planes, resulting in a LiO_3 and Nb termination (Cut 1′ and Cut 2′ in the picture). Cut 1′ and Cut 2′ represent the paraelectric reference phase to Cut 1 and Cut 2 of the ferroelectric phase in Fig. 5, Cut 3′ corresponds to the ferroelectric Cut 3

charge σ_S^{cut}has to be calculated with respect to a reference phase, as described by Eq. 5. Thereby, just as in case of the calculation of the volume spontaneous polarization via Berry phase, the correct choice of the (paraelectric) reference phase is crucial. In the case of a LN truncated bulk, it is relatively easy to find the cuts of the paraelectric phase corresponding to those of the ferroelectric phase. These are illustrated in Fig. 6 and denoted cut 1′, cut 2′ and cut 3′. Calculating the corresponding surface charge σ_P^{cut} and inserting it in Eq. 5, one obtains roughly the same value of the surface charge for all the three cuts, namely 0.65 ± 0.01 e/(1×1)-surface unit cell, see Table 1.

Next, σ_S^{cut} has been calculated with slabs containing a different number n of atomic layers. The dependence of σ_S^{cut} on the number of atomic layers is only marginal, see Table 2. However, the value of σ_S^{cut} for cells of infinite size can be

Table 2 Surface charge calculated at the positive LN(0001) for a Cut 1 termination with slabs containing a different number of atomic layers. σ_F^{cut}, σ_P^{cut} and σ_S^{cut} have the same meaning as in Table 1. All values in $e/(1 \times 1)$-surface unit cell

Layer number	18	24	30	36
σ_F^{cut}	−0.62	−0.64	−0.65	−0.66
σ_P^{cut}	−1.28	−1.30	−1.31	−1.31
σ_S^{cut}	0.66	0.66	0.66	0.65

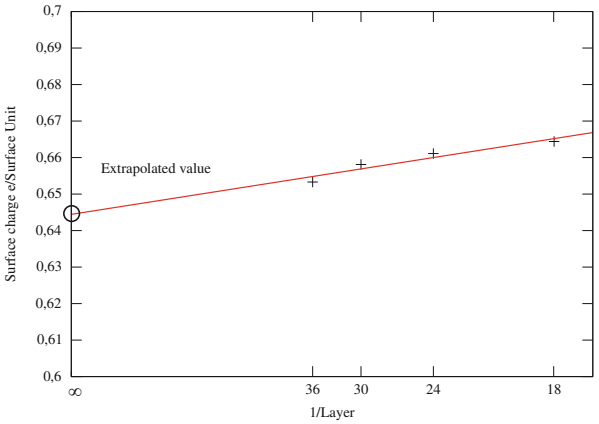

Fig. 7 Surface-charge density σ_S^{cut} as a function of the number n of atomic layer in the slab. The *solid line* is the linear interpolation of the calculated points, the extrapolated value for ideal infinite slabs is indicated

extrapolated plotting its dependence on $1/n$, as shown in Fig. 7. The extrapolated value of the surface charge $\sigma_S^{cut} = 0.64e/(1 \times 1)$ surface unit cell, corresponding to $0.46\,\mathrm{C/m^2}$ is somewhat lower, yet in reasonable agreement with the value expected from the bulk polarization. The deviation from the expected value might be traced back to the uncertainties introduced by the supercell approach as well as to a partial compensation by the electron transfer through the band gap in the calculation, and by the choice of partitioning the cell by Bader volumes. Thus, the calculated value does not allow for a quantitative prediction of the surface charge, however it will suffice for a qualitative discussion.

As a third step we calculated the surface charge for slabs of different periodicity. The calculated values are reported in Table 3. As expected, the charge σ_S^{cut} does not depend on the area of the unit cell used for the calculation.

Our method represents an important step towards the reconciliation of macroscopic and microscopic picture. The surface charge calculated with the three microscopic models is the same, and represents the polarization charge of an ideal bulk cut in our calculation.

After validating the method by application it to an ideal truncated bulk, we proceed with the calculation of the surface charge of realistic surfaces, which are

Table 3 Calculate surface charge ($e/(1\times1)$ unit cell) for the positive Cut 1 termination with slabs of different periodicity. σ_F^{cut}, σ_P^{cut} and σ_S^{cut} have the same meaning as in Table 1

Periodicity	1×1	$\sqrt{3}\times\sqrt{3}$	$\sqrt{7}\times\sqrt{7}$
σ_F^{cut}	−0.62	−0.65	−0.62
σ_P^{cut}	−1.28	−1.31	−1.28
σ_S^{cut}	0.66	0.66	0.66

characterized by relaxation and reconstructions. Levchenko et al. [20] predicted the phase diagram of the LN(0001) from ab initio thermodynamics, finding the stable terminations at the two surfaces to be rather temperature independent. In their work, however, only surfaces with 1×1 periodicity had been considered. Later, AFM measurements and DFT models including cells of different periodicity showed that different reconstructions might be formed at different temperature regimes [10]. Some of them might be inhibited by the presence of adsorbates and can only occur in vacuum. The corresponding phase diagram (now including reconstructed surfaces) has been calculated as a function of the chemical potentials of lithium and oxygen. As the goal of this investigation is to search for a correlation between surface charge and temperature, we first convert the phase diagram of the LN(0001) of Ref. [10] in a function of temperature and Li partial pressure. This can be done within the ideal gas approximation [25], as explained, e.g., in Ref. [13].

The result of this transformation is shown in Fig. 8 for the positive and negative LN Z-cut. A $\sqrt{3}\times\sqrt{3}$ reconstruction built by adding 2 Li atoms to the stable termination is formed at low temperatures at the positive face. With growing temperature, reconstructions containing less Li are formed, till after 1,000 K the 1×1 stable reconstruction predicted by Levchenko et al. [20] is restored. At the negative surface, a $\sqrt{7}\times\sqrt{7}$ reconstruction built adding 2 Li and 2 O atoms to the stable termination is formed at lower temperatures. With increasing temperatures, a further a $\sqrt{7}\times\sqrt{7}$ reconstruction built by adding 2 Li and a single O atoms and a $\sqrt{3}\times\sqrt{3}$ reconstruction obtained by adding a single oxygen atom to the stable termination are formed.

The succession of the surface reconstructions at different temperatures is shown in Table 4. The nominal charge added by the reconstruction at the positive side – also listed in the table – is a decreasing function of the temperature. However, the effective surface charge σ_S is not necessarily proportional to the nominal charge brought by the adsorbed species. Therefore, we calculate σ_S with the method previously illustrated.

At first, the relaxed 1×1 surface is considered. Differently from the truncated bulk termination, where the expected polarization charge is in principle known, there is no reference value for the clean, relaxed LN(0001) surfaces in vacuum. The only measurement of the surface charge of LN(0001) [23] we are aware of has been performed in air. The measured charge refers therefore to an adsorbate-covered surface. A relatively small surface charge of $140\,\mu C/m^2$ is measured for congruently melt, nominally undoped $LiNbO_3$ crystals. This is about $2{\cdot}10^{-4}$ smaller

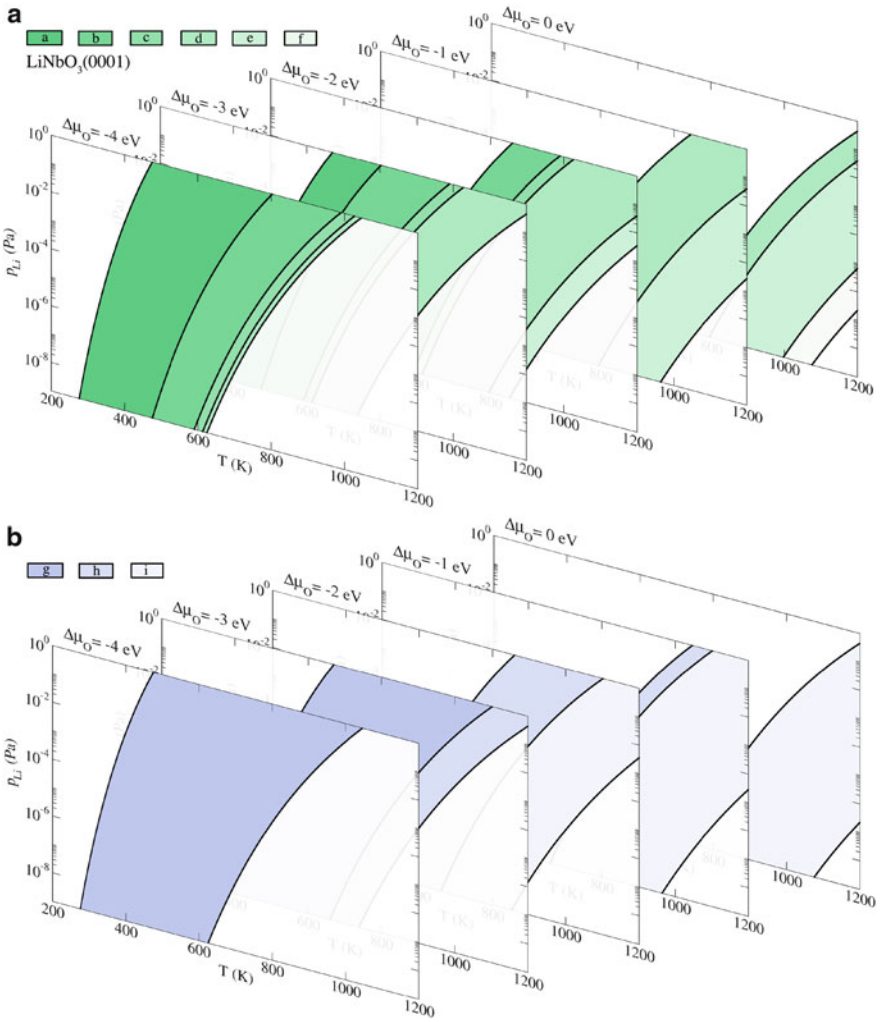

Fig. 8 Calculated phase diagram of the positive (*upper part*) and negative (*lower part*) LN(0001) surface as a function of temperature and pressure. The terminations (a)–(i) are explained in Table 4

than the spontaneous polarization of $0.71\,\mathrm{C/m^2}$, most likely due to the charge compensation by adsorbates.

The calculated surface charge of a $LiNbO_3$ slab terminated according to the stable surface structure (see Fig. 3) amounts to 0.104 $e/(1 \times 1)$ unit cell. This corresponds to about 16 % of the surface charge of the ideal ferroelectric bulk cut. This is in agreement with the predictions of Levchenko and Rappe [20]. In their work, they have proposed a model based on formal oxidation states to explain the stability of the preferred terminations of positive and negative surfaces by

Table 4 Calculated surface charge ($e/(1 \times 1)$ unit cell) for various LN Z-cut surfaces. The temperature range is assigned assuming a Li partial pressure of 10^{-8} Pa. Note that not all the surface reconstructions are allowed for arbitrary values of μ_O, as shown in Fig. 8. The data for positive and negative surfaces are given in the upper and lower part of the table, respectively

Periodicity	Termination	Stability range	Nominal charge	Surface charge σ_S
$\sqrt{3} \times \sqrt{3}$	+2Li (a)	250–450 K	0.66	+0.077
$\sqrt{7} \times \sqrt{7}$	+3Li (b)	450–600 K	0.43	−0.019
$\sqrt{3} \times \sqrt{3}$	+Li (c)	600–620 K	0.33	−0.052
$\sqrt{7} \times \sqrt{7}$	+2Li (d)	620–820 K	0.29	−0.041
$\sqrt{7} \times \sqrt{7}$	+Li (e)	820–1,050 K	0.14	−0.099
1×1	−(f)	1,050–1,150 K	0.00	−0.104
$\sqrt{3} \times \sqrt{3}$	+O (i)	680–1,150 K	0.66	+0.004
$\sqrt{7} \times \sqrt{7}$	+Li+O (h)	620–680 K	0.14	−0.071
$\sqrt{7} \times \sqrt{7}$	+2Li+O (g)	250–620 K	0.00	−0.087

passivation of surface charges with ions. According to this model, the surface charge of a truncated bulk LN(0001) surface is reduced by 80 % by the formation of the stable terminations, a value very close to the reduction by about 84 % calculated here. The experiment [23] shows that the surface charge must be compensated almost completely, because maintaining a non-zero surface charge is energetically unfavorable. The non-complete charge compensation resulting from the calculations is a result of limitations in the models, such as limited unit cell sizes, and most of all limited number of adsorbate types.

Next, we turn to reconstructed surfaces. The calculated values of the surface charge σ_S for reconstructions formed at different temperatures are complied in Table 4. The σ_S values for reconstruction at the positive face are calculated with the stable 1×1 termination at the negative side and vice versa. It is thus possible to estimate the efficiency of the single reconstructions in charge compensation. In all the investigated cases, the formation of an adatom-induced reconstruction yields a polarization charge reduction with respect to the stable 1×1 termination, thus stabilizing the surface. We find the lowering of the surface charge to be roughly proportional to the nominal charge of the adatoms. The $\sqrt{3} \times \sqrt{3}$ reconstruction formed by the addition of two Li-atoms at the positive side and the $\sqrt{3} \times \sqrt{3}$ reconstruction formed by the addition of one O-atom at the negative side (nominal additional charge of ± 0.66 electrons per 1×1 unit cell) lead to an overcompensation of the surface charge.

With increasing temperature surface terminations which only slightly reduce the polarization charge are favored. However, this does not mean that with increasing temperature a larger surface charge will be measured. Indeed, the surface charge in real samples will be a decreasing function of the temperature, as with increasing temperature the cations move closer to their paraelectric configuration, thereby reducing the net polarization. Thus, reconstructions with a minor impact on the surface charge will be sufficient for compensation. At temperatures above 1,200 K, the spontaneous polarization will be low enough that no surface reconstruction

is needed and the 1×1 periodicity is recovered. However, word of caution is in order here: The present calculations do not include thermal effects on the bulk polarization. Temperature effects enter exclusively, instead, via the chemical potentials of the surface constituents. This clearly affects the numerical accuracy of the calculated phase diagrams. Nevertheless, the present calculations strongly suggest the surface charge compensation as major driving force for the morphologic transformations observed on LN Z-cut surfaces.

4 Conclusions

A method for the calculation of the macroscopic surface charge within the periodically repeated slab approach has been proposed and applied to ferroelectric LN surfaces. The surface charge of an ideal truncated bulk is calculated to be $\sigma_S^{cut} = 0.46\,\mathrm{C/m^2}$. This value is reduced by about 84 % upon formation of the stable 1×1 surface structure found in Refs. [11, 20]. The surface reconstructions recently revealed by AFM techniques [10] further reduce the polarization charge, thus stabilizing the surface. Indeed, all the thermodynamically stable surface reconstructions lower the polarization charge. This strongly suggests that the surface charge compensation is the major driving force for the observed morphologic transformations. We want to remark that the present models represent clean surfaces of stoichiometric $LiNbO_3$. In congruent material the outgassing of LiO already at moderate temperatures ($\approx$600 K) severely deteriorates the crystalline quality and affects the surface composition. In addition, in real surfaces the presence of external adsorbates, surface defects and step edges will further reduce the surface charge.

Acknowledgements The calculations were done using grants of computer time from the Höchstleistungs-Rechenzentrum Stuttgart (HLRS) and the Paderborn Center for Parallel Computing (PC^2). The Deutsche Forschungsgemeinschaft is acknowledged for financial support.

References

1. Lee, T.C., Lee, J.T., Robert, M.A., Wang, S., Rabson, T.A.: Rabson, surface acoustic wave applications of lithium niobate thin films. Appl. Phys. Lett. **82**(2), 191 (2003)
2. Namkoong, G., Lee, K.K., Madison, S.M., Henderson, W., Ralph, S.E., Doolittle, W.A.: III-nitride integration on ferroelectric materials of lithium niobate by molecular beam epitaxy. Appl. Phys. Lett. **87**(17), 171107 (2005)
3. Stock, M., Dunn, S.: $LiNbO_3$ - A new material for artificial photosynthesis. IEEE Trans. Ultrason. Ferroelectr. Freq. Control **58**(9), 1988 (2011)
4. Stock, M., Dunn, S.: Influence of the ferroelectric nature of lithium niobate to drive photocatalytic dye decolorization under artificial solar light. J. Phys. Chem. C **116**(39), 20854 (2012)
5. Ferris, R., Yellen, B., Zauscher, S.: Ferroelectric Thin Films in Fluidic Environments: A new interface for sensing and manipulation of matter. Small **8**(1), 28 (2011)

6. Huang, S., Luo, J., Yip, H.L., Ayazi, A., Zhou, X.H., Gould, M., Chen, A., Baehr-Jones, T., Hochberg, M., Jen, A.K.Y.: Efficient poling of electro-optic polymers in thin films and silicon slot waveguides by detachable pyroelectric crystals. Adv. Mater. **24**(10), OP42 (2011)
7. Merola, F., Grilli, S., Coppola, S., Vespini, V., De Nicola, S., Maddalena, P., Čarfagna, C., Ferraro, P.: Reversible fragmentation and self-assembling of nematic liquid crystal droplets on functionalized pyroelectric substrates. Adv. Funct. Mater. **22**(15), 3267 (2012)
8. Li, D., Zhao, M.H., Garra, J., Kolpak, A.M., Rappe, A.M., Bonnell, D.A., Vohs, J.M.: Direct in situ determination of the polarization dependence of physisorption on ferroelectric surfaces. Nature Materials **7**(6), 473 (2008)
9. Rode, S., Hölscher, R., Sanna, S., Klassen, S., Kobayashi, K., Yamada, H., Schmidt, W.G., Kühnle, A.: Atomic-resolution imaging of the polar (0001) surface of $LiNbO_3$ in aqueous solution by frequency modulation atomic force microscopy. Phys. Rev. B **86**, 075468 (2012)
10. Sanna, S., Rode, S., Hölscher, R., Klassen, S., Marutschke, C., Kobayashi, K., Yamada, H., Schmidt, W.G., Kühnle, A.: Charge compensation by long-period reconstruction in strongly polar lithium niobate surfaces. Phys. Rev. B **88**, 115422 (2013)
11. Sanna, S., Schmidt, W.G.: Lithium niobate X-cut, Y-cut, and Z-cut surfaces from ab initio theory. Phys. Rev. B **81**, 214116 (2010)
12. Sanna, S., Gavrilenko, A.V., Schmidt, W.G.: Ab initio investigation of the $LiNbO_3$(0001) surface. Phys. Stat. Sol. (c) **7**(2), 145 (2010)
13. Sanna, S., Hölscher, R., Schmidt, W.G.: Polarization-dependent water adsorption on the $LiNbO_3$(0001) surface. Phys. Rev. B **86**, 205407 (2012)
14. Kresse, G., Furthmüller, J.: Efficient iterative schemes for ab initio total-energy calculations using a plane-wave basis set. Phys. Rev. B **54**(16), 11169 (1996)
15. Perdew, J.P., Yue, W.: Accurate and simple density functional for the electronic exchange energy: Generalized gradient approximation. Phys. Rev. B **33**(12), 8800 (1986)
16. Monkhorst, H.J., Pack, J.D.: Special points for Brillouin-zone integrations. Phys. Rev. B **13**, 5188 (1976)
17. Bengtsson, L.: Dipole correction for surface supercell calculations. Phys. Rev. B **59**, 12301 (1999)
18. Neugebauer, J., Scheffler, M.: Adsorbate-substrate and adsorbate-adsorbate interactions of Na and K adlayers on Al(111). Phys. Rev. B **46**, 16067 (1992)
19. Meyer, B., Vanderbilt, D.: Ab initio study of $BaTiO_3$ and $PbTiO_3$ surfaces in external electric fields. Phys. Rev. B **63**(20), 205426 (2001)
20. Levchenko, S.V., Rappe, A.M.: Influence of Ferroelectric Polarization on the Equilibrium Stoichiometry of Lithium Niobate (0001) Surfaces. Phys. Rev. Lett. **100**, 256101 (2008)
21. Vanderbilt, D., King-Smith, R.D.: Electric polarization as a bulk quantity and its relation to surface charge. Phys. Rev. B **48**, 4442 (1993)
22. Resta, R.: Modern theory of polarization in ferroelectrics. Ferroelectrics **151**(1), 49 (1994)
23. Johann, F., Soergel, E.: Quantitative measurement of the surface charge density. Quantitative measurement of the surface charge density, Appl. Phys. Lett. **95**, 232906 (2009)
24. Bader, R.F.W.: Atoms in Molecules – A Quantum Theory. Oxford University Press, Oxford (1990)
25. Landau, L.D., Lifshitz, E.M.: Statistical Physics, Part I, 3rd edn. Butterworth-Heinemann, Oxford (1981)